Supplementary material

Seizures initiate in zones of relative hyperexcitation in a zebrafish epilepsy model

Supplementary methods

Zebrafish preparation:

Mutant zebrafish larvae (*Tg(HuC:h2b-GCaMP6f) x Tg(Vglut2a:dsRed)*)[1-3] were used at 5 - 8 days after fertilization - the h2b-tag localizes GCaMP to the nucleus to disambiguate the site of origin of the signal by eliminating contamination from axonal and dendritic sources. After anesthetizing for 1 min in 0.1 g/L tricaine-methanesulfonate (MS222, VWR TCT0941- 025G), zebrafish were mounted dorsal-up in a 35 mm petri dish (35–1008, BD Falcon) lid containing a bed of 1.5 ml hardened 1% agarose (Invitrogen 15510-027) by embedding with droplets of 1.7% low temperature agarose (Sigma A0701-100G). Once the agarose hardened, a small incision in the skin was made (typically) above the neuropil in the right optic tectum for electrophysiology (see below). The agarose around the tail of the zebrafish was removed to monitor tail movement. The larva was then paralyzed by point incubation in droplets of 300 µM pancuronium bromide (Sigma P1918-10MG) and covered in 2.5-3 ml of glucose-free 10% (vol/vol) Evans medium (2.9 mM KCl, 1.2 mM MgCl2, 2.1 mM CaCl2, 134 mM NaCl, and 10mM HEPES, pH 7.8). Once tail movement ceased epileptiform activity was induced with bath application of 15 mM pentylenetetrazol (PTZ) (Sigma P6500-50G), which is more commonly used and effective than alternatives such as pilocarpine[4] and 4-Aminopyridine[5]. Recordings were performed within 2 hours after embedding zebrafish in agarose.

Electrophysiology

Local-Field Potential (LFP) recordings were acquired with metal microelectrodes during initial seizure characterization. One ~2-3 MΩ tungsten microelectrode (WE30013.0F3, Microprobes) was inserted in the optic tectum to record the LFP and a silver wire was placed in the Evans medium to serve as a reference. In some experiments, a second tungsten microelectrode was placed in either telencephalon or hindbrain region to confirm the global synchronous of ictal events. Electrophysiological recordings were amplified 1000x with a microelectrode amplifier (Model 1800, A-M Systems, Carlsborg, WA), digitized at 10K Hz using CED Power 1401, and stored with a computer running Spike2 software (Cambridge Electronic Design).

During calcium imaging, the LFP was recorded using a glass microcapillary to avoid obstructing fluorescence excitation and light collection. Capillaries (1B120F-4, WPI) were pulled to a fine tip with vertical puller (P30, Sutter Instruments) to a tip diameter of 2-3 μm. The capillaries were filled with 4M NaCl after front-loading molten agarose (1.7% Ultrapure Agarose, Thermo) to the tip to prevent diffusion of the electrode solution once inserted into the brain. When tested in Evans medium, these electrodes had a resistance of 1-3 MΩ. The electrode was inserted through incision in the skin into the neuropil of the right optic tectum. Recordings were made with a microelectrode amplifier (Model 1800, A-M Systems, Carlsborg, WA) using bandpass filtering (between 0.1 Hz and 1 kHz) at 10 kHz sampling rate and digitized using custom MATLAB code.

Correlation coefficient masks

During ictal events, GCaMP6f fluorescence in the image increases as the ictal event initiates and propagates through the brain. We first identified relevant brain areas by using the preprocessed GCaMP6f data to calculate pixelwise Pearson's correlation with the whole image average activity in the green GCaMP6f channel. To achieve this, we initially performed 2-dimensional Gaussian filtering on the imaging data (σ=2 pixels, ~4 micrometers) in MATLAB (*imgaussfilt*) and then smoothed individual pixels over time using a lowpass Butterworth filter (1st order, cutoff frequency of .2 Hz). These data are hereafter referred to as "smoothed images".

The individual pixel traces were then compared with the average of all pixel values in the image and a cutoff of 0.6 correlation (Pearson's *r*) was used to remove any pixels not sufficiently correlated with the average image activity. To remove any remaining noise, any smoothed pixels not connected in groups of at least 80 smoothed pixels were removed. The resulting image mask, called the correlation coefficient mask, simply represents the extent of brain that was involved in seizure events over individual files. This mask was applied in subsequent analyses of ictal event development.

Lag analyses for individual ictal events

Individual ictal events in the global signal were next detected in smoothed image series with a semi-automated method. First, general ictal event identification was performed: GCaMP6f fluorescence change was calculated as the frame-by-frame difference in the pixel-averaged fluorescence, and peaks were extracted with a minimum peak height of average plus 2 SD (a minimum peak-to-peak distance of 8 seconds was also included). Due to slight variations in noise or atypically spreading ictal events, in some data sets the standard deviation cutoff was increased (less than or equal to 3 SD) or performed on the average fluorescence activity instead of the difference. We then used 10 sec windows around those extracted times to find the peak first derivative activity. We note that these adjustments to the automated process are only included to produce accurate windows for finding ictal onsets and would not change the onset times. All individual ictal events were verified by visual examination of both the average GCaMP6f activity and the GCaMP6f image series videos.

We then defined analysis windows around these first derivative peaks and a global template for determination of relative onset times across the pixels. Our analysis window for each event began 10 s prior to this first derivative peak and extended 6 s past this peak. We then defined a global template for each event as the activity between the time 6 s prior to the peak and the peak.

For each ictal event, we then found the time of maximum correlation between the pixel trace and global template within the analysis window. Pixels not significantly correlated (Pearson's *r*, $p<0.05$) with the ictal event average or with a peak correlation below $r=0.6$ were excluded. When visualized as a heatmap this matrix provides a "lag map" where the ictal event activity began and spread across the imaging field of view. To remove any remaining noise, these lag maps were subsequently smoothed by a 2-D Gaussian kernel ($\sigma=6$ pixels, ~11 micrometers). To account for the line-scanning nature of our 2-photon images, a temporal transformation matrix was applied to shift every pixel by its true time in milliseconds (e.g., the first pixel of a single tiff image was scanned 256 ms prior to the pixel in the middle of the image). Note: when the 2D smoothing is applied to frames converted to milliseconds, and when single pixels' scan times are labelled my their ms-precision scan time, the gradations in lag maps will appear at less than 500 ms. This temporal precision is in appearance only, and our population analyses restrict data to full frame times.

From these lag maps, we used MATLAB's edge detection functions to extract the regions of the fish brain that were ictal event-active at the earliest 500 ms. We also applied an area requirement of 300 connected pixels (~0.5% of the 256x256 images) to exclude noise. These regions were used to measure which anatomical brain areas were most commonly invaded first by the ictal events. These regions were labelled the "initiation sites" in later single cell analyses. Other regions of the brain that were invaded later by the seizure are referred to as "propagation sites".

Correlations of these maps within fish were calculated as Pearson's *r* (across seizures within the same FOV) to measure similarity of seizure propagation within individual animals. These correlations were thus only calculated when more than one event occurred in a particular FOV within a fish.

A summary map (**Fig. 3D**) was created within an individual fish by setting a temporal cutoff (500 ms) for early activity in the lag map, creating a binary mask from this cutoff, and then averaging these binary masks over different ictal events. Thus, if a pixel is involved in 100% of the ictal event initiations of one fish then, it will receive a 1, if a pixel is involved in half of the ictal initiations it will receive a 0.5, etc. The correlation matrix (**Fig. 3B**) was calculated on ictal series with multiple seizures in FOVs containing all listed brain regions. Sequential and non-sequential seizure correlations were measured by Pearson's correlation coefficient (**Fig. 3C**).

To examine brain region involvement over different data sets, we compared the edges of initiation sites, per event, with the anatomical fish images (average fluorescence) and recorded the number of times that an initiation site contained a particular brain region, given that the brain region was present (e.g., if the habenula was not visible in a specific ictal series then it was not included in the analyses of early onsets). This data is shown in violin and schematic images (**Fig. 3E-F**), along with estimates of where seizures would occur if they initiated in a completely random manner. To calculate this, we took a subset of data (requiring at least 10 FOVs per brain region) and manually annotated brain regions and calculated their area as a fraction of the whole brain in the same FOV. We took the average and standard deviation of these estimates and show them as brackets in **Fig. 3E**, which indicate ranges where seizures would be expected to initiate if they were initiating in a completely random manner in the brain. Statistical comparisons between the fraction of initiations observed in brain regions versus the fraction of brain region in the FOVs are described in the Results.

Fine-scale template matching

Our standard global template matching procedure only specifies onset times with 500 ms resolution. To assess if any of our key results are biased by this resolution, we implemented a previously published procedure[6, 7] for fine-scale template matching that allowed improved specification of onset times. We first assessed how well this procedure can work in our setting using a realistic simulation where data is acquired from cells with known onset times.

For the simulation, we first generated a canonical response pattern by cubic interpolation at 1 kHz (*pchip*, MATLAB) of the global template from an individual seizure. We then used this signal to create simulated single cell activities by applying temporal offsets randomly to mimic cells with ictal onsets that varied across 500 ms (we did not simulate single cells' varying positions in the FOV). We also applied 1.5% noise to these traces, a value that we determined empirically from the range of noise values across cells in our data (1-2% was common). Data acquisition was simulated by then downsampling these activities to 2 Hz. We next generated a standard 2 Hz template by averaging the activity of these simulated cells (as done above for pixels), and then a fine-scale 32 Hz template by applying linear interpolation (*interp*) to this 2 Hz template. Template matching using these two cases was then caried out as described above (but taking 5% of the peak with a Pearson's correlation cutoff of at least r=0.8, as described in 'Single cell analysis'). We simulated this process 100 times (varying the random delays across cells) and compared actual and detected onset times from the two methods.

For re-analysis of the real data, we generated a 32-Hz linearly interpolated version of the original global template, then calculated when this fine-scale template was best correlated with individual pixel traces.

Single cell analysis

Single cells were extracted from the unsmoothed GCaMP6f images using an automated custom MATLAB algorithm with an added optional step that allowed for manually marking any single cells missed by our algorithm. First, within a single data set, the lowest quartile of GCaMP6f activity frames were used to create an average GCaMP6f image. Background subtraction was performed using structural element disks in MATLAB (with *imadjust*) and then an algorithm was used to iteratively step through all pixel luminance values (0 to 255) down to the lowest 20% and extract all connected regions containing at least 4 pixels (~2 microns/pixel), but removing any cells containing more than 40 pixels. All images were visually examined and any missed cells that could be visually determined were added manually in MATLAB with a custom script (using *imfreehand*), but typically fewer than 5 cells were added at this step. Finally, we applied a correlation threshold cutoff to remove any single cells whose activity was not at least r=0.3 correlated with the average activity of all the extracted cells. On average, our analyses extracted 351 seizure-active cells per image.

In separate cellular composition analyses, where we were interested in examining any detectable cells without requiring that they be seizure-active, we followed the above methods but used a lower Pearson's cutoff of r=0.1, which was low enough to include more cells than the above cutoff but high enough to exclude artifacts (such as occur on skin edges and near the animal's eyes).

To separate putative inhibitory (expressing only GCaMP) and excitatory cell types (co-expressing DsRed and GCaMP in VGlut2+ cells) we took the red intensity values from individual cells and plotted their histogram. These histograms are characterized by two peaks: the first peak, lower red values, denotes the GCaMP-positive cells that do not co-express DsRed (putative inhibitory interneurons); the second peak, higher red intensity values, denotes the GCaMP-positive cells that also co-express DsRed (putative excitatory neurons). These histograms were fit by a dual gaussian mixture model (**Fig. S6**), and the mean and standard deviation of both component gaussians were extracted (*fitgmdist* in MATLAB). The cutoff used in our study for labeling a cell as excitatory was two standard deviations past the first gaussian's mean. In some cases, artifacts from the zebrafish skin, eyes, or a tilt in the animal's body could affect these histograms. In those cases, the histogram fitting was performed regionally by manually selecting anatomical regions (applying MATLAB's *imfreehand*) and then performing the dual gaussian fit. All images were visually examined after cell type dissociation by plotting cell types on composite red/green images of the larval zebrafish to verify appropriate labelling by the algorithm. In two data sets we could not extract E vs I cell type differences (due to either imaging or fluorophore labelling technical difficulties), so the ictal events in those data series were not included in our E:I single cell analyses leaving N=167 ictal events.

Seizure onsets

In order to compare results across animals and seizure events, we extracted ictal onset times from each ictal event for all single cells. General ictal events were found above (see Lag Analyses), but for single cell analyses we sought to determine the exact time of cell onsets relative to a population onset. Thus, we applied a similar correlation method as the pixelwise lag analyses above but with global templates that were centered around the peak second derivative of single cell population activity, the time of fastest recruitment of individual neurons to a seizure event.

Single cell involvement in seizures was determined by identifying the times at which individual cells became significantly involved in the ictal events (**Fig. S4**). To find these times in single neurons we filtered the cell GCaMP6f profiles by temporally smoothing in 2 s windows (boxcar average) and then compared these traces in time windows around ictal event onsets that were found in the lag analyses above.

Global response templates in this analysis were created by first finding the peak second derivative of the population activity during an ictal event. This point served as the center of the global template. We next stepped forward in time to the peak first derivative of the population activity; this was the end point of the global template. We then took an equal amount of time backwards from the center of the template; this was the start point of the global template. Thus, we created a template centered on the peak acceleration point of the ictal event, a time that more accurately represents true ictal event onset compared to other methods of cutoffs such as half-height or 2-standard deviations above the mean. We refer to this peak acceleration time of the population activity as the ictal onset.

Next, we found the peak linear correlation (Pearson's *r*) between this template and individual cell fluorescence traces in a window from 8 s before the beginning of the template and 3 s after the end of the global template. This wide temporal window was important because our method of global template creation depends on the rise time of the ictal event: slowly evolving

ictal events will have longer templates than faster events. (Note: the correlation window used for single cell onsets was 11 seconds plus the length of the global template, making it a window approximately equal to the 16 sec window used in lag analyses above). Our algorithm required that a single cell be at least r=0.8 correlated with the global template to be included as having an onset in the ictal event, a strict requirement to reduce the chance of erroneous single cell onset classifications (our main findings were robust to this r cutoff varying from 0.7, 0.8, and 0.9, **Fig. S7**). The onset time for a single cell was classified as the time where it reached 5% of peak correlation (above the 0.8 cutoff) with the global template. This 5% requirement was included because many cells displayed wide peaks of correlation with the global template: taking the earliest peak correlation most accurately represented the onset of a single cell in the ictal event. Because some cells displayed small fluctuations in fluorescence that coincided with ictal onsets, when cells exhibited more than one r=0.8 peak during the time window analyzed, we took the later r=0.8 peak to prevent erroneous early-onset classifications. Finally, all individual cell onsets were temporally adjusted for the 2-photon system's scanning (as done for the pixelwise lag analysis, shifting by the pixel scan time from the cell centroid), and the population activity was temporally corrected by 256 ms (the midpoint time of the frame scan). This method was applied to all data sets and all cells regardless of E or I classification.

When temporally aligning data we used the average ictal onset time calculated across all cells significantly recruited to each individual seizure, a procedure analogous to the relative times calculated in our lag analyses above. Thus, data are displayed relative to this time zero point.

Inter-ictal periods were defined as all times outside of ictal events (after PTZ application). We classified the termination of ictal events as the point at which the average fluorescence activity returned to its value at the second derivative onset, which was used to separate ictal vs interictal time periods for later analyses.

Supplementary figures

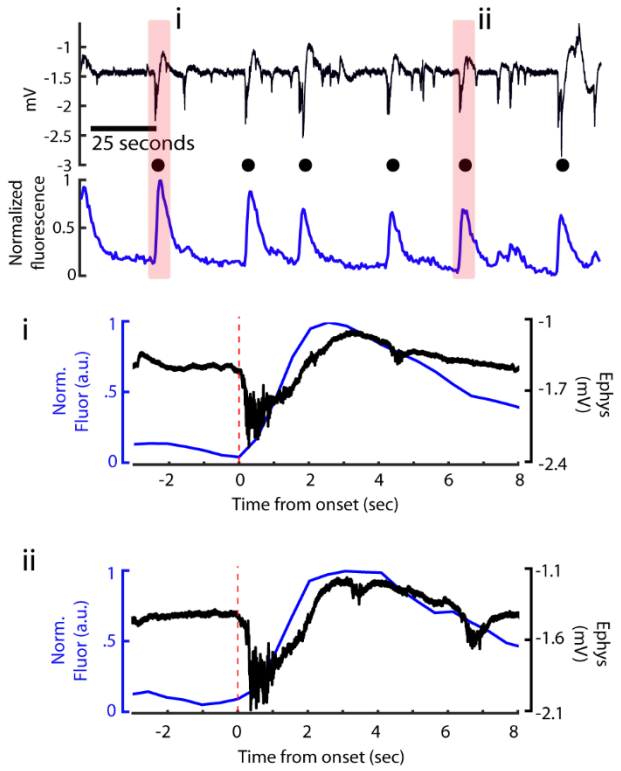

Figure S1. Identical timing of ictal events in calcium and electrophysiological signals. A sample series of ictal events is shown from **Figure 1**, with two seizures highlighted (pink). The first event is shown in higher temporal magnification (i), as well as the fifth event (ii). A 2 Hz notch filter was applied to the electrophysiological signals in the bottom panels, and the calcium activity is taken from the entire imaging frame. Our onset detection method was applied to all seizures (red dashed line).

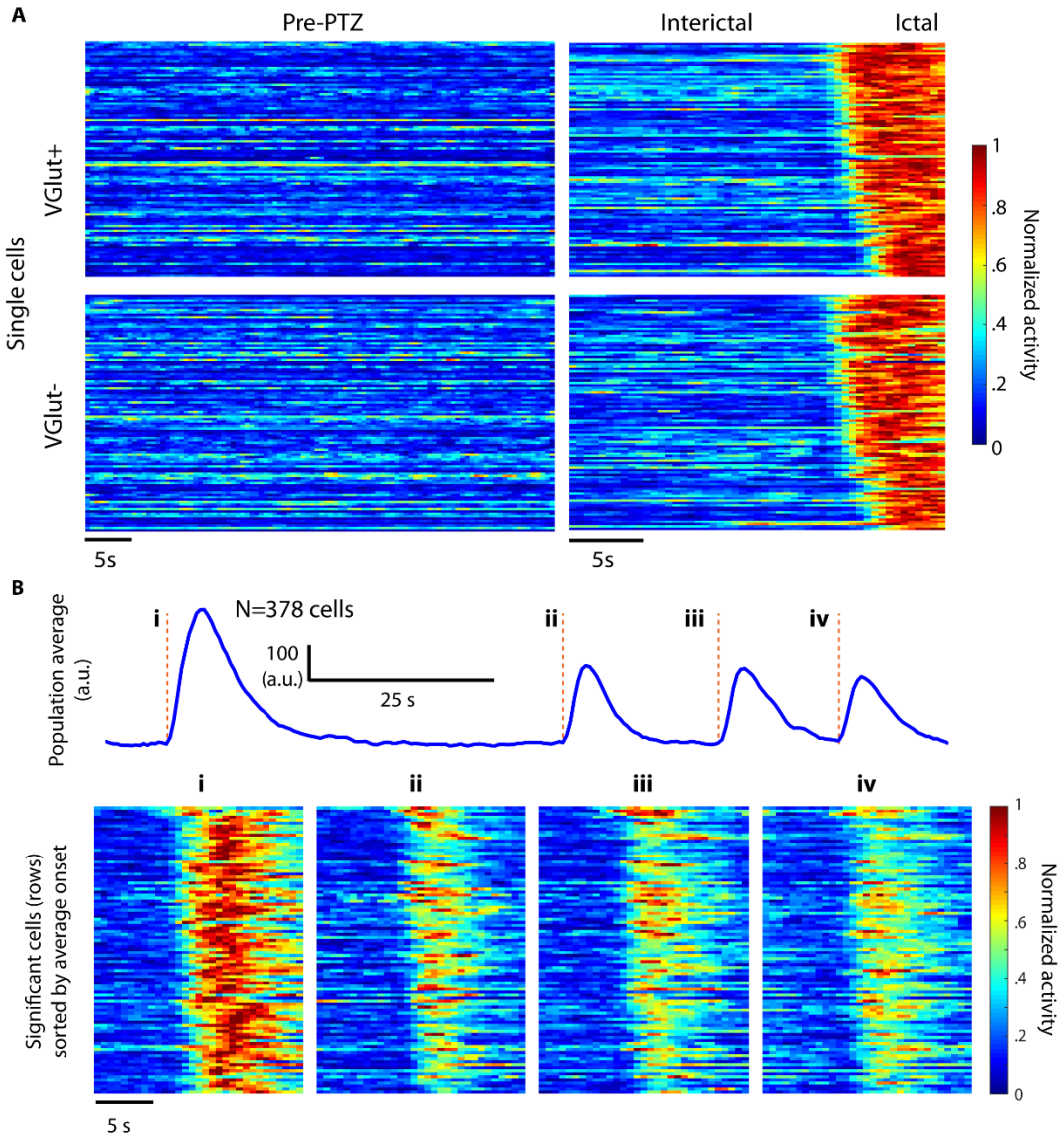

Figure S2. Single cell activity. (**A**) Individual cell activity is shown (rows) for the same cells prior to PTZ administration (*left*) and interictal activity prior to an ictal event (*right*) after PTZ administration. Excitatory and inhibitory cell types are shown separately and sorted by detected onset time within this ictal event. (**B**) Top: cell population activity demonstrates a series of four ictal events; Bottom: single cell activity during these events is shown sorted by average onset across events.

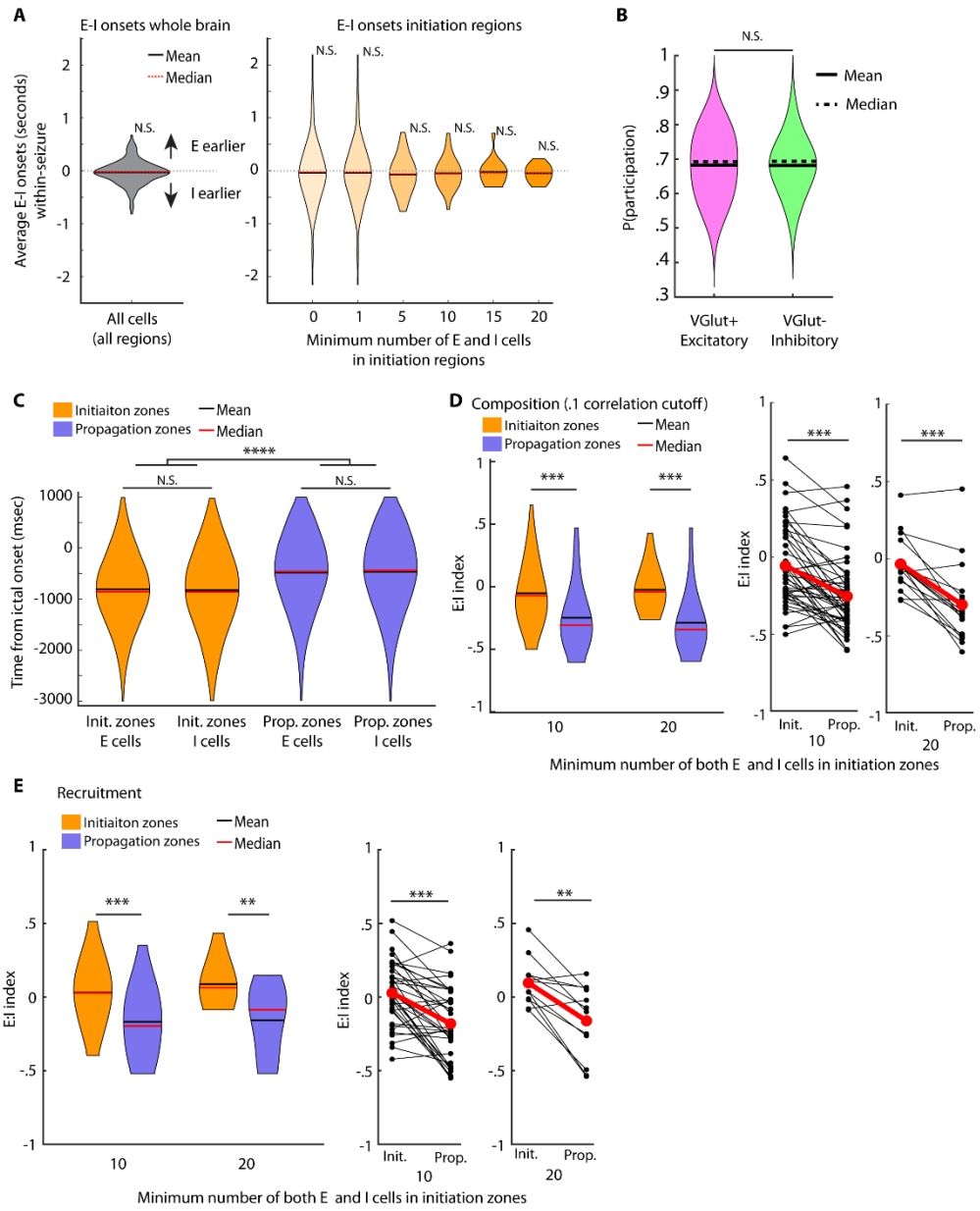

Figure S3. Associated with Figure 4 E:I and onset timing. (**A**) Left: the difference in average onset time between excitatory and inhibitory cell populations is shown (positive values indicate earlier excitatory cell onset) for the whole brain. Right: same analysis for initiation zones. Initiation zones are divided into varying sizes (All seven violins: N=167, N=167, N=101, N=62, N=36, N=18, N=12 ictal events; none were significant by α=.05, Wilcoxon signed-rank test). (**B**) Probability of participation was calculated across all E and I cells that participated in more than one seizure (N=40 data series with at least 2 seizures, 159 seizures total; N.S. α=.05, Wilcoxon rank-sum test). (**C**) Recruitment times between E and I cell types (N=1264, N=1135, N=12143, N=14992; N.S., α=.05, Wilcoxon rank-sum test) and between initiation and propagation sites (**** p<.0001, Wilcoxon signed-rank test). (**D**) Number of E and I cells detected in regions that

were determined to be initiation and propagation zones, regardless of whether these cells participated in seizure events, shown across multiple size cutoffs (N=49, N=18, Wilcoxon signed-rank test, *** p<.001). For all data (167 seizures), with no cell count cutoffs, E:I composition in initiation regions was -0.069 +/- 0.042 (SEM), while E:I composition in propagation regions -0.232 +/- 0.024, corresponding to a roughly 29% increase in E:I ratio in the initiation zone relative to the propagation zone across all seizures. (**E**) Number of E and I cells recruited in initiation and propagation zones shown across multiple size cutoffs (N=36, N=12, p<.001, Wilcoxon signed-rank test, ** p<.01, *** p<.001). For all data (167 seizures), with no cell count cutoffs, E:I recruitment in initiation regions was 0.034 +/- 0.043 (SEM), while E:I recruitment in propagation regions was -0.162 +/- 0.022, a significant difference corresponding to a roughly 40% increase in E:I ratio in the initiation zone relative to the propagation zone across all seizures.

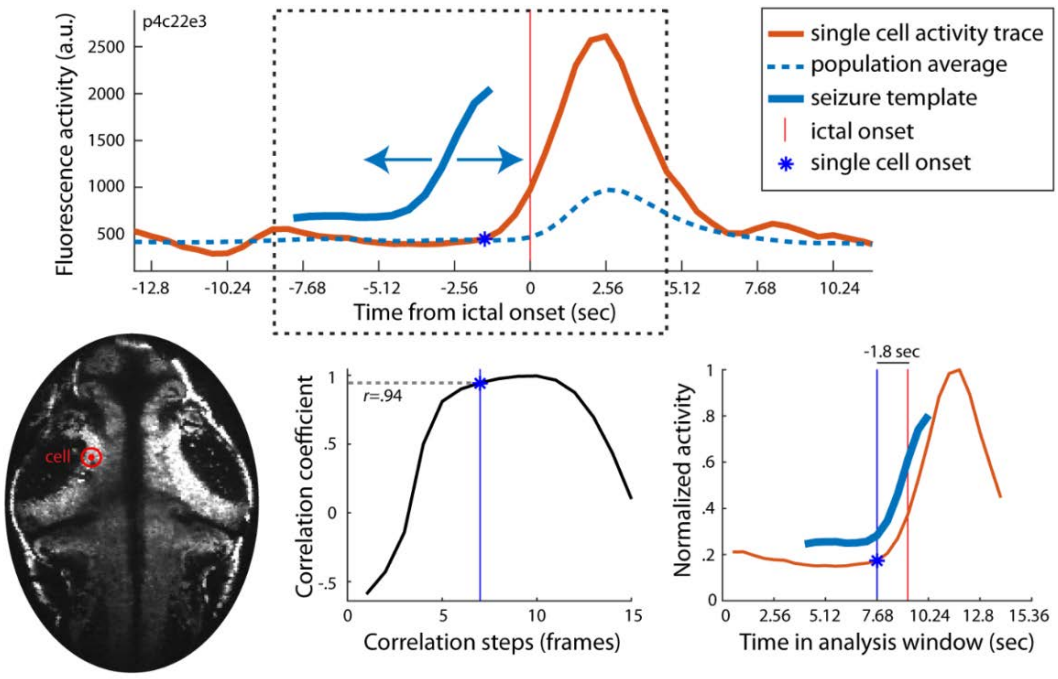

Figure S4. Single cell onset detection. Ictal events were detected from global (all cells) activity, and a template of global activity was created around the peak second derivative of this trace. Top: this template was slid along single cell activity traces to determine the estimated onset of the single cell based on its correlation with the global template (see Methods). Bottom, left to right: the single cell location in the fish, the correlation at each step of the analysis with the best fit location marked, and the template aligned with the single cell onset estimate. This single cell's onset was ~1.8 seconds earlier than the population ictal onset.

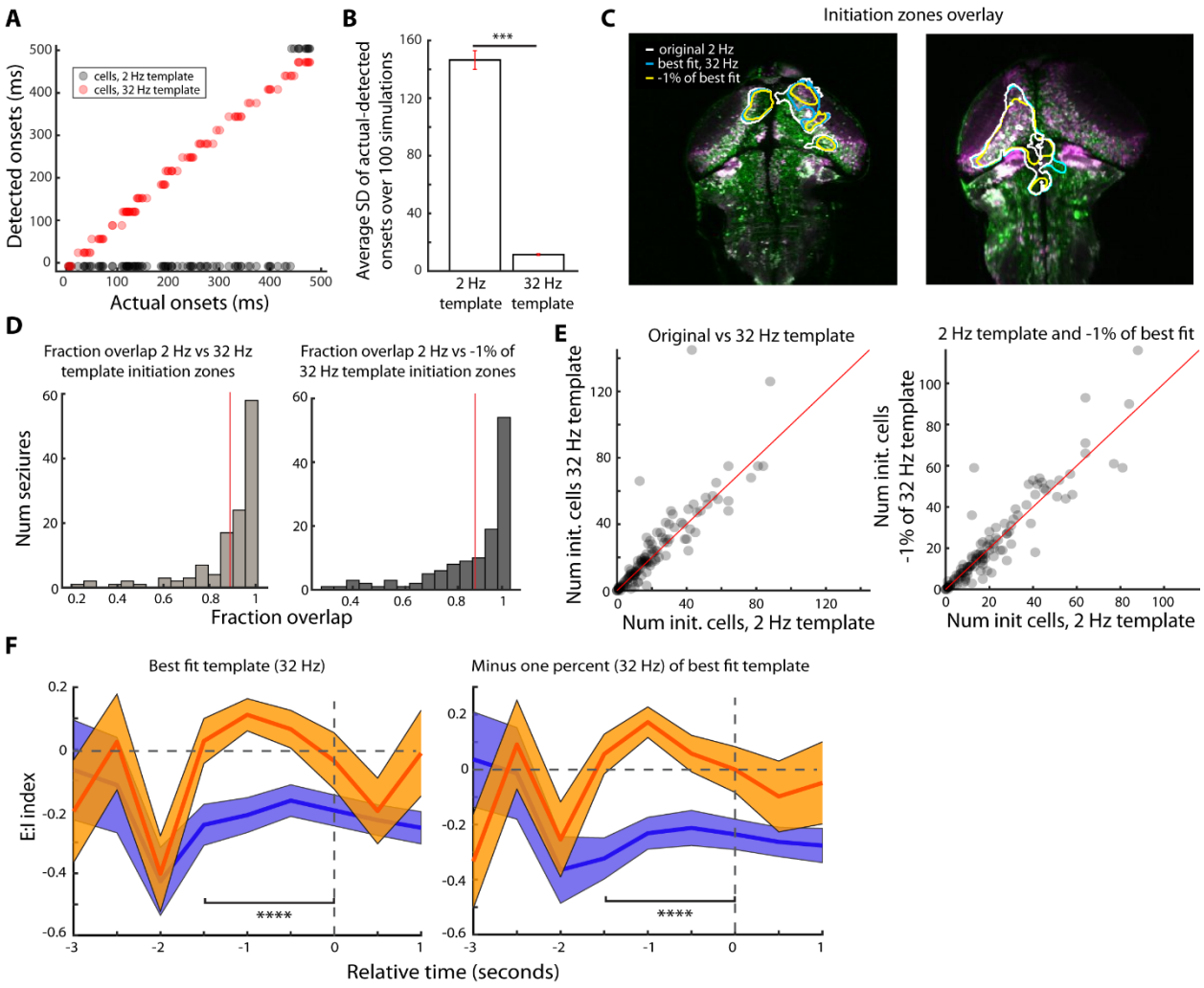

Figure S5. Fine-scale template matching. (**A**) Detected vs actual onset times for simulated single-cell activities using templates defined either at 2 or 32 Hz resolution. (**B**) Results from 100 simulations that randomly varied ictal onsets of 100 artificial cells showing the average variation (SD) between true onset time and detected onset time using 2 Hz and 32 Hz templates. ($p<0.001$, t-test, N=100). (**C**) Two example seizures' initiation zones are shown in two different fish, showing initiation zone outlines calculated from 2- and 32- Hz templates (white and blue, respectively), and a -1% of peak 32-Hz template fit to assess sensitivity (yellow). (**D**) Overlap of initiation zones was calculated for both 32-Hz templates and a -1% version of the template-matching (mean, red lines, and SD of overlap for 2 vs 32 Hz templates =0.89 +/- 0.16 and 0.86 +/- 0.16 for the -1% case, N=167 seizures). (**E**) Numbers of cells in initiation zones were recalculated with the new high-resolution templates. Linear regression produced a slope of .80 with 95% CI=[0.75 0.86] for original vs 32 Hz templates; slope=0.91 with 95% CI=[0.86 0.95] for 2 Hz templates vs the -1% case. (**F**) A main finding, higher E:I index values in initiation zones vs propagation zones, was not changed by applying a 32-Hz template (left) or the -1% version of the same procedure (**** $p<0.0001$, Wilcoxon signed-rank test, N=39 events (left) and N=34 events (right)).

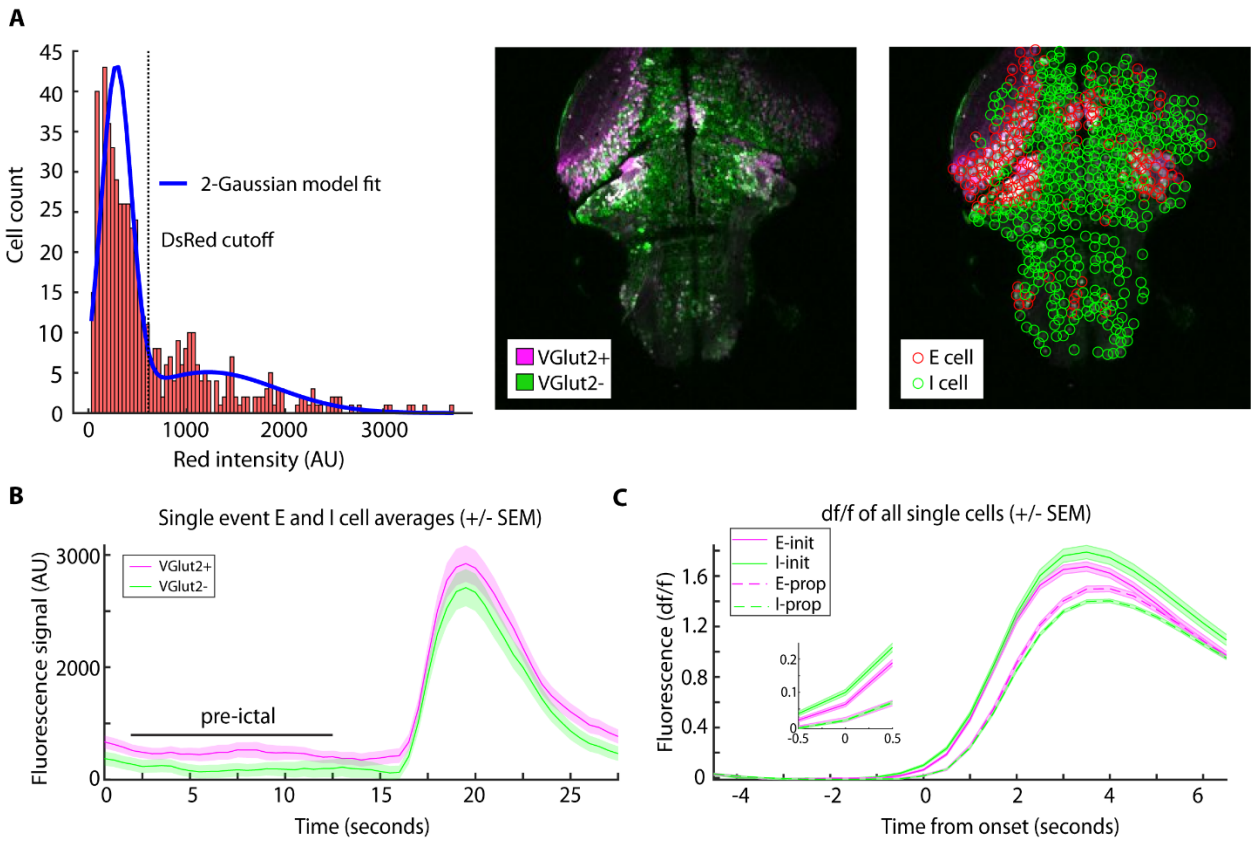

Figure S6. Excitatory and inhibitory cell identification. (**A**) For each fish a 2-Gaussian mixture model was fit to the histogram of red channel intensities of cells (left) to quantitatively separate the cell types (center and right panels). (**B**) Average fluorescence signal was similar between VGlut2+ and VGlut2- cell types during individual ictal events (individual seizure here, VGlut2+ N=170, VGlut2- N=152). (**C**) Fluorescence change (df/f) was similar within E and I cell types in initiation and propagation zones when averaged across all seizures (N=123 events; E-init N=1324, I-init N=1210, E-prop N=9541, I-prop N=12189).

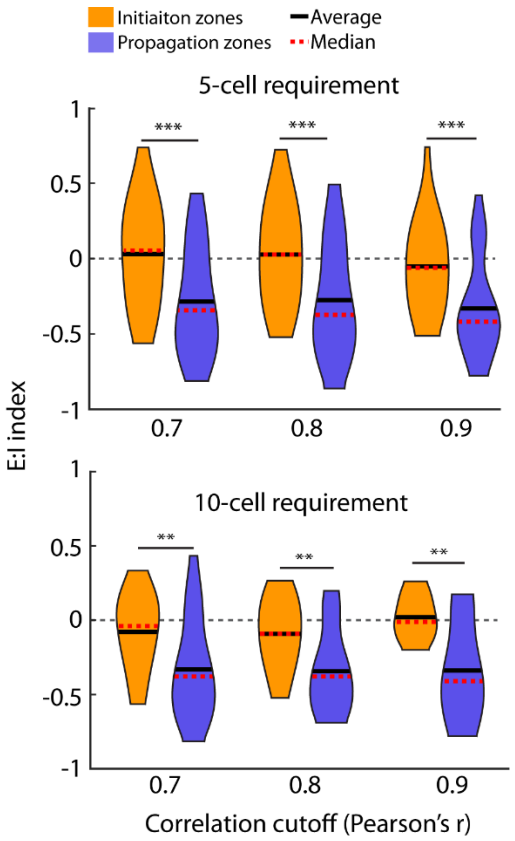

Figure S7. Excitation:Inhibition differences between initiation and propagation zones are robust to variation in single cell correlation cutoffs. We varied the correlation cutoff required for a cell to be counted as recruited to seizures in a subset of 50 seizures taken across all fish in our single cell analyses. E:I index was significantly different between initiation and propagation zones regardless of whether the correlation cutoff was set to r=0.7, 0.8, or 0.9. This effect was also robust across cell count cutoffs, requiring either 5 E and 5 I cells (top panel, N=36, 34, 24, seizures respectively) or 10 E and 10 I cells (bottom panel, N=21, 19, 12 seizures, respectively). Wilcoxon signed-rank test, ** $p<0.01$, *** $p<0.001$.

References (supplemental)

1. Higashijima S, Mandel G, Fetcho JR. Distribution of prospective glutamatergic, glycinergic, and GABAergic neurons in embryonic and larval zebrafish. J Comp Neurol 2004;480:1-18.
2. Dunn TW, Mu Y, Narayan S, et al. Brain-wide mapping of neural activity controlling zebrafish exploratory locomotion. Elife 2016;5.
3. Satou C, Kimura Y, Hirata H, Suster ML, Kawakami K, Higashijima S. Transgenic tools to characterize neuronal properties of discrete populations of zebrafish neurons. Development 2013;140:3927-3931.
4. Verdugo CD, Myren-Svelstad S, Aydin E, et al. Glia-neuron interactions underlie state transitions to generalized seizures. Nat Commun 2019;10.
5. Liu J, Baraban SC. Network Properties Revealed during Multi-Scale Calcium Imaging of Seizure Activity in Zebrafish. Eneuro 2019;6.
6. Ramsey MC, Pitz RW. Template matching for improved accuracy in molecular tagging velocimetry. Exp Fluids 2011;51:811-819.
7. Wang S, Si JH, Shao J, Hu ZY, Ye JF, Liu JR. Two-dimensional interferometric Rayleigh scattering velocimetry using multibeam probe laser. Opt Eng 2017;56.